ELSEVIER

Comput. Methods Appl. Mech. Engrg. 190 (2001) 2771–2787

Computer methods in applied mechanics and engineering

www.elsevier.com/locate/cma

Finite element modeling of electro-mechanically coupled analysis for ferroelectric ceramic materials with defects

Daining Fang [a,*], Ai Kah Soh [b]

[a] *Department of Engineering Mechanics, Tsinghua University, Beijing 100084, People's Republic of China*
[b] *Department of Mechanical Engineering, University of Hong Kong, Hong Kong, People's Republic of China*

Received 13 July 1999

Abstract

In light of the equations of static mechanical and electrical equilibrium of ferroelectric materials, the functional is presented by using the principle of virtual work in this paper. Formulation of the electro-mechanically coupled finite element analysis for ferroelectric materials with defects has been described in details. The effect of depolarization in ferroelectrics has been taken into account in the formulation. In addition, various electric boundary conditions on the crack surfaces in ferroelectric ceramics are implemented in the finite element procedure developed. Thus, the current finite element method (FEM) has been extended to account for the impermeable, permeable and conducting cracks, by considering that the crack gap is filled with homogenous dielectric media. As an example, the crack propagation of a double edge notched specimen of a PZT-5H ferroelectric ceramic with exact electric boundary conditions on the crack surfaces is analyzed.

1. Introduction

A review of ferroelectric ceramic materials has been provided by Jaffe et al. [1]. Most piezoelectric materials are made of ferroelectric crystals such as lead zirconate titanate (PZT) and barium titanate ($BaTiO_3$). Ferroelectrics belong to a subgroup which, when in the form of a single domain, processes a spontaneous polarization that can be reversed by applying a high electric field or a large stress. When a ferroelectric ceramic is subjected to an electric field, the cations and anions displace somewhat in the opposite directions, giving rise to both a polarization and a distortion. Such effects form the basis of electro-mechanical sensors, transducers and actuators [2]. Most ferroelectrics are also linearly piezoelectric when they are operating around the spontaneous polarization. However, depolarization occurs when they are subjected to excessive electric field or stress. On the other hand, ferroelectric ceramics are brittle and susceptible to cracking at all scales from domains to devices. The concerns of structural reliability of various electro-mechanical devices call for a better understanding of the mechanisms of piezoelectric fracture in ferroelectric materials. Theoretical studies of fracture in piezoelectric solids have been made by many researchers, such as Parton [3], Cherepanov [4], Deeg [5], Park and Herrmann [6], McMeeking [7,8], Park [9], Sosa [10,11], Suo et al. [12], Suo [13], Wang [14], Duun [15], Kumar and Singh [16], Park and Sun [17], Zhang and Tong [18], Gao et al. [19] and many others. However, for these materials, due to the unexplained discrepancies between the theory and experiments, even the basic criterion of fracture remains a point of controversy [19]. To-date, the work performed has been mainly focused on seeking the analytical

* Corresponding author.
E-mail address: fangdn@mail.tsinghua.edu.cn (D. Fang).

0045-7825/01/$ - see front matter
PII: S0045-7825(00)00269-3

solution when simple boundary conditions were implemented. Parton [3] considered the problem of a finite crack at the interface of a piezoelectric medium and a conductor subjected to a far field tension. He obtained a generalized Griffith formula involving the critical crack length. Deeg [5] used Green's function method, by modeling the crack as a collinear dislocation and charge dipole line, to study the fracture problem in piezoelectric material. Sosa and Pak [11] analyzed a three-dimensional semi-infinite crack in a transversely isotropic piezoelectric medium by means of the eigenfunction expansions and found that both the stress and electric field have $1/\sqrt{r}$ singularity at the crack tip. Despite the fact that many researchers have put in significant efforts to seek the crack propagation criterion, no suitable one has been found. Some researchers' conclusions are contrary to other results. Park and Sun [17] obtained a close form solution for three types of cracks in infinite media. They found from the potential release rate that the applied electric field always retards the crack propagation, which does not agree with experiment results. However, the mechanical strain energy release rate (MSERR) does agree with that of their experiments. Hence, they concluded that MSERR is a good criterion for predicting crack propagation. In addition, they also found that an applied negative electric field retards crack propagation.

As the electro-mechanical devices developed become more complex in geometry, analysis of such devices is even more complicated due to the electro-mechanical coupling effect of the ferroelectric materials. Thus, there is a necessity to formulate numerical methods capable of analyzing the macroscopic coupling response of the system, and simulating the failure behavior (e.g., fracture, fatigue) of the materials and structures. Some attempts have been made by researchers in the aforementioned area of interest. Wang and Shen [20] have established the variational theory for thermal, electric, magnetic and elastic materials. Hom and Shankar [21,22] have developed a finite element method (FEM) to analyze the eletrostric deformation in electro-strictors. Kumar and Singh [23] have employed the finite element package ABAQUS to analyze the crack propagation in piezoelectric ceramics. They found that an applied negative electric field might aid the crack propagation, which is contrary to Park and Sun's conclusion [17].

Another problem that is of great interest to researchers is the crack surface electrical boundary conditions (CSEBC) [7,12,15,24,25]. Due to its much simpler mathematical treatment, the impermeable assumption of a hole or crack filled with air or vacuum, associated with its boundary free of forces and electric surface charge, was assumed in the aforementioned articles. However, McMeeking [7] and Duun [15] have pointed out that the singular behavior of the electric field at the tip of a sharp crack is an anomaly caused by the impermeable assumption. In fact, they have found that the magnitude of the field remains bounded by the permittivities of the piezoelectric material and gas enclosed by the crack. Parton [3] took a crack to be a traction-free, but permeable, slit. This is to say, the electric potential and the normal component of the electric displacement are continuous across the slit. However, Suo [12] has commented that these permeable boundary conditions cannot be defended on physical grounds. This is particularly true for ferroelectric ceramics, for which the permittivity is 10^3 times higher than the environment (e.g., air or silicone oil). A crack may be thought of as a low-capacitance medium carrying a potential drop. McMeeking [7,8] modeled cracks in dielectrics containing a conducting fluid. In this case, the crack becomes electrically conducting such that the electric potential on the crack surface equals zero. The CSEBC increase the complication and difficulties in the fracture analysis of ferroelectric materials. Although efforts have been made to theoretically figure out the effect of CSEBC on piezoelectric fracture, to the authors' best knowledge, the numerical analysis of fracture in piezoelectric or ferroelectric materials for different CSEBC has not been reported so far.

The purpose of this paper is to present an electro-mechanically coupled finite element approach for analyzing deformation and fracture of ferroelectric ceramic materials with defects. In this paper, by employing the basic equilibrium equations, the electro-mechanical potential function is obtained which enables the FEM formulation. The effect of depolarization in ferroelectrics has been taken into account in the formulation. In addition, various electrical boundary conditions on the crack surfaces of ferroelectric ceramics are also considered in the finite element procedure developed. Thus, the current FEM can be extended to account for the impermeable, permeable and conducting cracks, by considering that the crack gap is filled with homogenous dielectric media. As an example, the crack propagation of a double edge notched specimen of a PZT-5H ferroelectric ceramic with exact electric boundary conditions on the crack surfaces is analyzed. The work on the nonlinear finite element analysis of ferroelectric materials, subjected to the ferroelectric and ferroelastic domain switching, is in progress and will be reported in the near future.

2. Governing equations for static electro-mechanics

Ferroelectric materials are approximately linear when an applied electric field or stress is small compared to the depoling field. Thus, the stress $\boldsymbol{\sigma}$, strain $\boldsymbol{\varepsilon}$, electric displacement $\boldsymbol{D}$, and electric field $\boldsymbol{E}$ obey the following linear constitutive relations:

$$\sigma_{ij} = C_{ijkl}\varepsilon_{kl} - e_{ijk}E_k, \tag{1a}$$

$$D_i = e_{ijk}\varepsilon_{jk} + k_{ij}E_j, \tag{1b}$$

where C_{ijkl}, e_{ijk} and k_{ij} are the elastic and piezoelectric constants and dielectric permittivities, respectively. These constants are material specific. For example, the constants for PZT and $BaTiO_3$ are of the orders: $C_{ijkl} \sim 10^{11}$ N/m^2, $k_{ij} \sim 10^{-8}$ F/m, $e_{ijk} \sim 10^{1}$ C/m^2. Assume that a ferroelectric ceramic is subjected to a field of displacement $\boldsymbol{u}$ and electric potential ϕ. Based on the geometric compatibility requirement, the strain and the electric fields can be derived from the gradients as follows:

$$\varepsilon_{ij} = \frac{1}{2}\left(u_{i,j} + u_{j,i}\right), \tag{2a}$$

$$E_i = -\frac{\partial\phi}{\partial x_i}. \tag{2b}$$

Across an interface between two materials, we have

$$n_i(\sigma_{ij}^{+} - \sigma_{ij}^{-}) = T_j, \tag{3a}$$

$$n_i(D_i^{+} - D_i^{-}) = -P^{\mathrm{e}}, \tag{3b}$$

where P^{e} is electric charge and T_j is force; and n_i is the unit normal of the surface. The mechanical equilibrium requires that the stress tensor is divergence-free inside a material, and the electrical equilibrium requires that the electric displacement vector be divergence-free in a dielectric:

$$\sigma_{ij,i} + f_j = 0, \tag{4a}$$

$$D_{i,i} = -p^{\mathrm{e}}, \tag{4b}$$

where f_j and p^{e} are body force and electric charge, respectively. Given a ferroelectric ceramic, the mechanical and electric boundary conditions are

$$\sigma_{ij}n_i = \bar{T}_j \quad \text{on } S^{\sigma}, \tag{5a}$$

$$D_i n_i = \bar{p}^{\mathrm{e}} \quad \text{on } S^{D}, \tag{5b}$$

$$u_i = \bar{u}_i \quad \text{on } S^{u}, \tag{5c}$$

$$\phi = \bar{\phi} \quad \text{on } S^{\phi}, \tag{5d}$$

where u_i, ϕ, $\bar{p}^{\mathrm{e}}$, $\bar{T}_j$ and n_i are the displacement vector, electric potential, surface electric charge, surface force and normal of the surface, respectively. S^{σ}, S^{D}, S^{u} and S^{ϕ} refer to the stress, electric displacement, displacement and electric potential boundaries, respectively.

Based on the principle of virtual work, for the real solution of the system in the domain V with the boundary ∂V, the following variational equation exists:

$$\int_V \left[\left(\sigma_{ij,i} + f_j\right)\delta u_j + (D_{i,i} - p^{\mathrm{e}})\delta\phi\right] \mathrm{d}V - \int_{S^{\sigma}} \left(\sigma_{ij}n_i - \bar{T}_j\right)\delta u_j \,\mathrm{d}S - \int_{S^{D}} \left(D_i n_i - \bar{p}^{\mathrm{e}}\right)\delta\phi \,\mathrm{d}S = 0. \tag{6}$$

Applying the generalized Green–Gauss theorem, the first term of the left-hand side in Eq. (6) can be written as

$$\int_V \left[\left(\sigma_{ij,i}+f_j\right)\delta u_j+(D_{i,i}-p^e)\delta\phi\right]\mathrm{d}V=\int_V\left(-\sigma_{ij}\delta u_{i,j}-D_i\delta\phi_{,i}\right)\mathrm{d}V+\int_V(f_i\delta u_i+p^e\delta\phi)\,\mathrm{d}V+\int_{S^\sigma}\bar{T}_j\delta u_j\,\mathrm{d}S+\int_{S^D}\bar{p}^e\delta\phi\,\mathrm{d}S. \tag{7}$$

Considering the constitutive equations (1a) and (1b) and the geometry equations (2a) and (2b) the first term of the right-hand side of Eq. (7) can be written as

$$\int_V\left(-\sigma_{ij}\delta u_{i,j}-D_i\delta\phi_{,i}\right)\mathrm{d}V=\int_V\left(-\sigma_{ij}\delta\varepsilon_{ij}+D_i\delta E_i\right)\mathrm{d}V=\delta\left[\int_V-\frac{1}{2}C_{ijkl}\varepsilon_{kl}\varepsilon_{ij}+e_{ijk}E_k\varepsilon_{ij}+\frac{1}{2}k_{ij}E_iE_j\right]\mathrm{d}V. \tag{8}$$

Thus, the potential of the system in domain V with its boundary ∂V is as follows:

$$\Pi=\int_V\left(\frac{1}{2}C_{ijkl}\varepsilon_{ij}\varepsilon_{kl}-e_{ijk}\varepsilon_{ij}E_k-\frac{1}{2}k_{ij}E_iE_j\right)\mathrm{d}V-\int_V(f_iu_i-p^e\phi)\,\mathrm{d}V-\int_{S^\sigma}\bar{T}_iu_i\mathrm{d}S-\int_{S^D}\bar{p}^e\phi\,\mathrm{d}S. \tag{9}$$

Of all the fields ($\boldsymbol{u}$, ϕ) satisfying Eqs. (5c) and (5d), the solution renders [12]

$$\delta\Pi=0, \tag{10}$$

Suo et al. [12] pointed out that since the electric enthalpy, $\Psi(\boldsymbol{\varepsilon},\ \boldsymbol{E})$, is not positive definite, it is not necessary to minimize the solution field, Π. In addition, although the relevant energy function, Ψ, is indefinite, uniqueness can be stated for a fairly general class of nonlinear materials in the case of small deformation. Thus, development of an isoparametric finite element, which is of displacement-electric potential type, can be carried out. A finite element procedure will be proposed in the next section by using the aforementioned variational principle. The proposed element has four degrees of freedom, u_1, u_2, u_3, ϕ, at each node.

3. Formulation of electro-mechanical coupled FEM

By considering the mechanical and electrical equilibrium equations, the following symmetric relationship can be established:

$$u_i\sim\phi,\quad \varepsilon_{ij}\sim E_i,\quad \sigma_{ij}\sim D_i. \tag{11}$$

A finite element of displacement-electric potential type can then be developed. Taking the nodal displacement u_i and nodal potential ϕ as basic variables, the displacement and potential at point $P(\xi_1,\xi_2,\xi_3)$ in the element can be interpolate as

$$u_i=\sum_{j=1}^{n}N_ju_i^{(j)}=N_{ik}a_k^{(u)},\quad k=1,2,3,\ldots,3n, \tag{12a}$$

$$\phi=\sum_{j=1}^{n}N_j\phi^{(j)}=N_ja_j^{(\phi)}, \tag{12b}$$

where n is the number of nodes of an element; N_j denotes the interpolation functions; and $\boldsymbol{a}^{(u)}$ and $\boldsymbol{a}^{(\phi)}$ are the nodal displacement and potential vectors, respectively, which are defined as

$$\boldsymbol{a}^{(u)}=\left[u_1^{(1)}\quad u_2^{(1)}\quad u_3^{(1)}\quad\cdots\quad u_1^{(n)}\quad u_2^{(n)}\quad u_3^{(n)}\right]^{\mathrm{T}}, \tag{13a}$$

$$\boldsymbol{a}^{(\phi)} = \left[\, \phi^{(1)} \quad \cdots \quad \phi^{(n)} \,\right]^{\mathrm{T}}. \tag{13b}$$

Therefore,

$$u_{i,j} = \frac{\partial u_i}{\partial x_j} = \frac{\partial u_i}{\partial \xi_r}\frac{\partial \xi_r}{\partial x_j} = u_{ir}J_{rj}^{-1} = N_{ik,r}a_k^{(u)}J_{rj}^{-1} = \tilde{B}_{ijk}^{(u)}a_k^{(u)}, \tag{14}$$

where $\tilde{B}_{ijk}^{(u)} = N_{ik,r}J_{rj}^{-1}$, thus,

$$\varepsilon_{ij} = \frac{1}{2}\left(u_{i,j} + u_{j,i}\right) = \frac{1}{2}\left(N_{ik,r}J_{rj}^{-1} + N_{jk,r}J_{ri}^{-1}\right)a_k^{(u)} = \tilde{B}_{ijk}^{(u)}a_k^{(u)} \tag{15}$$

and

$$\phi_{,i} = \frac{\partial \phi}{\partial x_i} = \frac{\partial \phi}{\partial \xi_r}\frac{\partial \xi_r}{\partial x_i} = N_{j,r}a_j^{(\phi)}J_{ri}^{-1} = \tilde{B}_{ij}^{(\phi)}a_j^{(\phi)}. \tag{16}$$

Eqs. (15) and (16) can take the matrix form:

$$\varepsilon = \begin{Bmatrix} \varepsilon_{11} \\ \varepsilon_{22} \\ \varepsilon_{33} \\ \varepsilon_{44} \\ \varepsilon_{55} \\ \varepsilon_{66} \end{Bmatrix} = \begin{Bmatrix} \tilde{B}_{11} \\ \tilde{B}_{22} \\ \tilde{B}_{33} \\ \frac{1}{2}\left(\tilde{B}_{12} + \tilde{B}_{21}\right) \\ \frac{1}{2}\left(\tilde{B}_{13} + \tilde{B}_{31}\right) \\ \frac{1}{2}\left(\tilde{B}_{23} + \tilde{B}_{32}\right) \end{Bmatrix} \boldsymbol{a}^{(u)} = \boldsymbol{B}^{(u)}\boldsymbol{a}^{(u)}, \tag{17}$$

$$\boldsymbol{E} = -\begin{Bmatrix} E_1 \\ E_2 \\ E_3 \end{Bmatrix} = -\begin{Bmatrix} \tilde{B}_1^{(\phi)} \\ \tilde{B}_2^{(\phi)} \\ \tilde{B}_3^{(\phi)} \end{Bmatrix} \boldsymbol{a}^{(\phi)} = \boldsymbol{B}^{(\phi)}\boldsymbol{a}^{(\phi)} \tag{18}$$

in which $\boldsymbol{B}^{(u)}$ is a $6 \times 3n$ matrix and $\boldsymbol{B}^{(\phi)}$ is a $3 \times n$ matrix. Substituting Eqs. (17) and (18) into the first term of Eq. (9), we obtain

$$\begin{aligned}
&\int_V \left(\frac{1}{2}C_{ijkl}\varepsilon_{ij}\varepsilon_{kl} - e_{ijk}\varepsilon_{ij}E_k - \frac{1}{2}k_{ij}E_iE_j\right)\mathrm{d}V \\
&= \sum_e \int_{V^e} \left(\frac{1}{2}\boldsymbol{a}^{(u)^{\mathrm{T}}}\boldsymbol{B}^{(u)^{\mathrm{T}}}\boldsymbol{C}\boldsymbol{B}^{(u)}\boldsymbol{a}^{(u)} - \boldsymbol{a}^{(u)^{\mathrm{T}}}\boldsymbol{B}^{(u)^{\mathrm{T}}}\boldsymbol{e}\boldsymbol{B}^{(\phi)}\boldsymbol{a}^{(\phi)} - \frac{1}{2}\boldsymbol{a}^{(\phi)^{\mathrm{T}}}\boldsymbol{B}^{(\phi)^{\mathrm{T}}}\boldsymbol{d}\boldsymbol{B}^{(\phi)}\boldsymbol{a}^{(\phi)}\right)\mathrm{d}V \\
&= \sum_e \frac{1}{2}\boldsymbol{a}^{(u)^{\mathrm{T}}}\int_{V^e}\boldsymbol{B}^{(u)^{\mathrm{T}}}\boldsymbol{C}\boldsymbol{B}^{(u)}\,\mathrm{d}V\boldsymbol{a}^{(u)} - \sum_e \boldsymbol{a}^{(u)^{\mathrm{T}}}\int_{V^e}\boldsymbol{B}^{(u)^{\mathrm{T}}}\boldsymbol{e}\boldsymbol{B}^{(\phi)}\,\mathrm{d}V\boldsymbol{a}^{(\phi)} - \sum_e \frac{1}{2}\boldsymbol{a}^{(\phi)^{\mathrm{T}}}\int_{V^e}\boldsymbol{B}^{(\phi)^{\mathrm{T}}}\boldsymbol{d}\boldsymbol{B}^{(\phi)}\,\mathrm{d}V\boldsymbol{a}^{(\phi)} \\
&= \sum_e \left(\frac{1}{2}\boldsymbol{a}_e^{(u)^{\mathrm{T}}}\boldsymbol{K}_e^{(u)}\boldsymbol{a}_e^{(u)} - \frac{1}{2}\boldsymbol{a}_e^{(u)^{\mathrm{T}}}\boldsymbol{K}_e^{(u\phi)}\boldsymbol{a}_e^{(\phi)} - \frac{1}{2}\boldsymbol{a}_e^{(\phi)^{\mathrm{T}}}\boldsymbol{K}_e^{(u\phi)^{\mathrm{T}}}\boldsymbol{a}_e^{(\phi)} - \frac{1}{2}\boldsymbol{a}_e^{(\phi)^{\mathrm{T}}}\boldsymbol{K}_e^{(\phi)}\boldsymbol{a}_e^{(\phi)}\right).
\end{aligned} \tag{19}$$

Define the generalized element nodal displacement vector as

$$\boldsymbol{a}_e = \left[\, \boldsymbol{a}_e^{(u)^{\mathrm{T}}} \quad \boldsymbol{a}_e^{(\phi)^{\mathrm{T}}} \,\right]^{\mathrm{T}}. \tag{20}$$

Thus,

$$\frac{1}{2}\boldsymbol{a}_e^{(u)^{\mathrm{T}}}\boldsymbol{K}_e^{(u)}\boldsymbol{a}_e^{(u)} = \frac{1}{2}\boldsymbol{a}_e^{\mathrm{T}}\begin{bmatrix} \boldsymbol{K}_e^{(u)} & 0 \\ 0 & 0 \end{bmatrix}\boldsymbol{a}_e, \tag{21a}$$

$$\frac{1}{2}\boldsymbol{a}_e^{(u)^{\mathrm{T}}}\boldsymbol{K}_e^{(u\phi)}\boldsymbol{a}_e^{(\phi)} = \frac{1}{2}\boldsymbol{a}_e^{\mathrm{T}}\begin{bmatrix}0 & K_e^{(u\phi)}\\ 0 & 0\end{bmatrix}\boldsymbol{a}_e, \tag{21b}$$

$$\frac{1}{2}\boldsymbol{a}_e^{(\phi)^{\mathrm{T}}}\boldsymbol{K}_e^{(u\phi)^{\mathrm{T}}}\boldsymbol{a}_e^{(u)} = \frac{1}{2}\boldsymbol{a}_e^{\mathrm{T}}\begin{bmatrix}0 & 0\\ K_e^{(u\phi)^{\mathrm{T}}} & 0\end{bmatrix}\boldsymbol{a}_e, \tag{21c}$$

$$\frac{1}{2}\boldsymbol{a}_e^{(\phi)^{\mathrm{T}}}K_e^{(\phi)}\boldsymbol{a}_e^{(\phi)} = \frac{1}{2}\boldsymbol{a}_e^{\mathrm{T}}\begin{bmatrix}0 & 0\\ 0 & K_e^{(\phi)}\end{bmatrix}\boldsymbol{a}_e. \tag{21d}$$

Therefore, the first term of Π in Eq. (9) can be written as

$$\sum_e \frac{1}{2}\boldsymbol{a}_e^{\mathrm{T}}\begin{bmatrix}\boldsymbol{K}_e^{(u)} & -\boldsymbol{K}_e^{(u\phi)}\\ -\boldsymbol{K}_e^{(u\phi)^{\mathrm{T}}} & -\boldsymbol{K}_e^{(\phi)}\end{bmatrix}\boldsymbol{a}_e = \sum_e \frac{1}{2}\boldsymbol{a}_e^{\mathrm{T}}\boldsymbol{K}'_e\boldsymbol{a}_e. \tag{22}$$

In the above formulation, the generalized displacement vector is not in the sequence of nodal number. Therefore, in programming the row and column of $\boldsymbol{K}'_e$, some adjustment must be made to meet the requirement for assembling the global stiffness matrix. It can be seen that the diagonal elements of the global stiffness matrix are not always positive. This means that the global stiffness matrix is not always positive definite. In solving the ordinary static and dynamic problems, this will not give rise to any difficulty in obtaining numerical solutions. Whereas, in solving eigenvalue problems, the aforementioned weakness can be overcome by adding a positive value to the diagonal element involved. Therefore, the non-positive global stiffness matrix will not introduce any difficulty in the FEM solution.

4. Depolarization model for ferroelectric ceramics

As mentioned in the previous sections, analogies may be drawn between the mechanical and electrical variables in terms of their roles in the above equations, such as $u_i \sim \phi,\ \varepsilon_{ij} \sim E_i,\ \sigma_{ij} \sim D_i,\ T_j \sim P^{\mathrm{e}}$. However, for ferroelectric materials, it is $\boldsymbol{\varepsilon}$ and $\boldsymbol{D}$ together that define the physical distortion. Therefore, an energy function, $\Phi(\boldsymbol{\varepsilon}, \boldsymbol{D})$, exists and is given by

$$\mathrm{d}\Phi = \sigma_{ij}\,\mathrm{d}\varepsilon_{ij} + E_i\,\mathrm{d}D_i, \tag{23}$$

where Φ is convex in the $(\boldsymbol{\varepsilon}, \boldsymbol{D}, \Phi)$-space for stable materials. As mentioned before, for the finite element procedure, we have to formulate the theory based on displacement $\boldsymbol{u}$ and potential ϕ. A more convenient energy function called the electric enthalpy, $\Psi(\boldsymbol{\varepsilon}, \mathbf{E})$, is defined by

$$\Psi = \Phi - E_i D_i. \tag{24}$$

A Legendre transformation shows that

$$\mathrm{d}\Psi = \sigma_{ij}\,\mathrm{d}\varepsilon_{ij} - D_i\,\mathrm{d}E_i. \tag{25}$$

The materials deform when they are subjected to an electric field and polarize when stresses are applied. Linear piezoelectrics can be described in a quadratic form when the applied loads are small compared to the poling field

$$\Psi = \frac{1}{2}C_{ijkl}\varepsilon_{ij}\varepsilon_{kl} - \frac{1}{2}d_{rs}E_rE_s - e_{rij}E_r\varepsilon_{ij}. \tag{26}$$

The stress and the electric displacement are given by

$$\sigma_{ij} = \partial\Psi/\partial\varepsilon_{ij}, \quad D_i = -\partial\Psi/\partial E_i. \tag{27}$$

From Eqs. (26) and (27), the constitutive relation for linear piezoelectrics can be obtained as follows:

$$\sigma_{ij} = C^{\mathrm{E}}_{ijmn}\varepsilon_{mn} - e_{nij}E_n, \tag{28a}$$

$$D_i = e_{imn}\varepsilon_{mn} + k^{\varepsilon}_{in}E_n, \tag{28b}$$

where C^{E}_{ijmn}, e_{imn} and k^{ε}_{in} are elastic and piezoelectric constants and dielectric permittivities, respectively. Note that the superscripts refer to the testing condition. For instance, C^{E}_{ijmn} is measured at a constant electric field and k^{ε}_{in} is measured at a given strain. It should be noted that Ψ is not convex in the $(\boldsymbol{\varepsilon}, \boldsymbol{E}, \Psi)$-space [12]. This is to say it has such a saddle point that the solution field need not minimize the functional, Π, as given in Eq. (9).

By the similar approach employing the energy Φ, an alternative set of constitutive equations using σ and $\boldsymbol{E}$ as controlling quantities can be expressed as

$$\varepsilon_{ij} = M^{\mathrm{E}}_{ijmn}\sigma_{mn} + d_{mij}E_m, \tag{29a}$$

$$D_j = d_{jmn}\sigma_{mn} + k^{\sigma}_{jm}E_m, \tag{29b}$$

where M^{E}_{ijmn}, d_{ijk} and k^{σ}_{in} are the compliance moduli (measured in a constant electric displacement), the piezoelectric coefficients and the dielectric constant (measured at a constant stress), respectively. In general, according to the different controlling quantities, there are four types of the piezoelectric constitutive equations in which the material constants satisfy the following relations [26]:

$$\begin{aligned} d_{mij} &= e_{mkl}M^{\mathrm{E}}_{klij} = k^{\sigma}_{mn}g_{nij}, \quad e_{mij} = d_{mkl}C^{\mathrm{E}}_{klij} = k^{\varepsilon}_{mn}h_{nij}, \\ g_{mij} &= h_{mkl}M^{D}_{klij} = \beta^{\sigma}_{mn}d_{nij}, \quad h_{mij} = g_{mkl}C^{D}_{ijkl} = \beta^{\varepsilon}_{mn}e_{nij}, \end{aligned} \tag{30}$$

where g_{nij} and h_{mij} are the piezoelectric coefficients and β_{in} the dielectric constants. C_{ijmn} and k_{in} are the 'inverse' of M_{ijmn} and β_{in}, respectively.

The properties of ferroelectric ceramics are a composite of the properties of the individual grains. Each grain of the ceramics is a single crystal. Fig. 1 illustrates the crystal structures of the most widely concerned ferroelectric material, ABO_3 ($BaTiO_3$ is an example). The ABO_3 perovskite contains an A^{2+} ion at each corner of the unit cell, a B^{4+} ion at the center of the unit cell, and an O^{2-} ion at the center of each face.

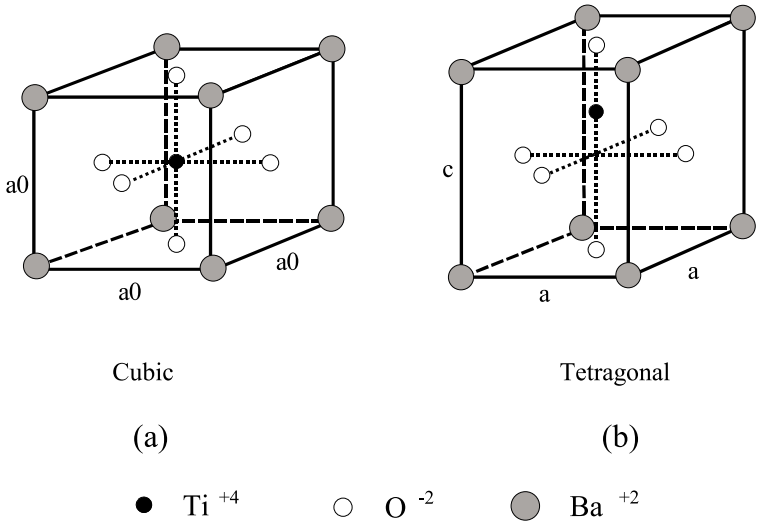

Fig. 1. The crystal structures of barium titanate ($BaTiO_3$). The paraelectric phase is nonpolar. The ferroelectric phase is polar and the Ti^{4+} is off the cell center.

Above the Curie temperature about 130°C, the crystal is cubic, and the ions lie symmetrically in the unit cell: both the positive and the negative charge centers coincide with the cube center. The cubic phase is paraelectric phase and the crystal is nonpolar. At the room temperature or a temperature between 0°C and 130°C, the crystal is tetragonal, and the ions lie asymmetrically in the unit cell; the positive and the negative charge centers are separated from each other. That is, the tetragonal unit cell has an ionic dipole moment due to the displacement of the central Ti^{4+} ion relative to the surrounding O^{2-} ions. The tetragonal phase is ferroelectric phase and the crystal is poled. The polarization is, by definition, the dipole moment per unit volume. The coupling between the strain and the electric field is a consequence of this polar structure. The crystal structure is changed during phase transformation. The *a*- and *b*-axes contract and the *c*-axis expands. The structure deformation induces a spontaneous strain. The structure deformation also causes a relative displacement of ions and induces a spontaneous electric polarization along the *c*-axis. The spontaneous strain in the local coordinate is

$$[\varepsilon_{ij}^*] = \begin{bmatrix} (a-a_0)/a_0 & & \\ & (a-a_0)/a_0 & \\ & & (c-a_0)/a_0 \end{bmatrix}. \tag{31}$$

The spontaneous electric polarization in the local coordinate is

$$\left[D_i^*\right] = \left[P_i^*\right] = [\,0 \quad 0 \quad P_s\,], \tag{32}$$

ε_{ij}^* and p_i^* can be ascertained for a given material at a certain temperature. For example, at the room temperature, the tetragonal phase of barium titanate has lattice constants $a = 3.992$ Å and $c = 4.032$ Å, and a polarization $P_s = 0.26\ \mathrm{C/m^2}$ [12]. The intrinsic material property makes ferroelectric ceramics useful as sensors and actuators, and the ability to change the direction of polarization by an applied electric field or stress, can lead to depolarization [27–30]. The stress and electric field levels sufficient to cause depolarization are relatively low. This fact should be well understood by the device designers [29,30]. In general, most of the piezoelectric ceramics has ferroelectric crystals. These crystals have to be polarized first, by applying an electric field in excess of the coercive field, before any application in order to get the piezoelectric properties. Due to poling, an overall remanent polarization $\bar{P}^{\mathrm{r}}$ exists to align the polarization of each of the grains. In applications, the applied positive (negative) electric field is usually defined as parallel (opposite) to the poling direction. A compressive stress or a large negative electric field may lead to a reduction of the polarization of the material [30,31]. Therefore, after unloading, there exists a remanent polarization in the ferroelectric ceramics. Thus, it is of great interest to investigate the effect of the remanent polarization on the electro-mechanical fields near an elliptic void or crack of a ferroelectric medium. The following simple constitutive relations have been derived by the authors [32–34] and other researchers [30] to account for the effect of the depolarization

$$\varepsilon_{ij} = M_{ijmn}^{\mathrm{E}}\sigma_{mn} + d_{mij}E_m, \tag{32a}$$

$$D_j = d_{jmn}\sigma_{mn} + k_{jm}^{\sigma}E_m + \bar{P}^{\mathrm{r}}, \tag{32b}$$

where the remanent polarization equals to the fully poled saturation magnitude of that of the poled ceramic when it is not subjected to the external loads, i.e., $\bar{P}^{\mathrm{r}} = \bar{P}_s^{\mathrm{r}}$. After unloading an applied load, the value of the remanent polarization of the ceramic can be expressed as [34]

$$\bar{P}^{\mathrm{r}} = \frac{1}{8\pi^2}\int_0^{\pi}\int_0^{2\pi}\int_0^{2\pi} P^*(\theta,\varphi,\psi)\sin\theta\,\mathrm{d}\psi\,\mathrm{d}\varphi\,\mathrm{d}\theta, \tag{33}$$

where θ, φ, ψ are three Eular angles relative to the domain orientation. In order to employ the constitutive equation (32) in the finite element procedure, these angles must be rewritten in a form using ε and $\boldsymbol{E}$ as controlling quantities. Based on the relation that C_{ijmn} and k_{in} are the 'inverse' of M_{ijmn} and β_{in}, respectively, and by using Eq. (30), (32) can be expressed as

$$\sigma_{ij} = C_{ijmn}^{\mathrm{E}}\varepsilon_{mn} - e_{nij}E_n, \tag{34a}$$

$$D_i = e_{imn}\varepsilon_{mn} + \tilde{k}_{in}E_n + \bar{P}_i^{\mathrm{r}}, \tag{34b}$$

where

$$\tilde{k}_{in} = k_{in}^{\sigma} - d_{ijk}e_{jkn}. \tag{35}$$

According to Eqs. (34a) and (34b) the functional in Eq. (9) can be modified by

$$\begin{aligned}\Pi = &\int_V \left(\frac{1}{2}C_{ijkl}\varepsilon_{ij}\varepsilon_{kl} - e_{ijk}\varepsilon_{ij}E_k - \frac{1}{2}\tilde{k}_{ij}E_iE_j + \bar{P}_i^{\mathrm{r}}E_i\right)\mathrm{d}V \\ &- \int_V (f_iu_i - p_e\phi)\mathrm{d}V - \int_{S^{\sigma}} \bar{T}_iu_i\mathrm{d}S \; - \int_{S^D} \bar{p}^{\mathrm{e}}\phi\,\mathrm{d}S.\end{aligned} \tag{36}$$

5. Crack surface electrical boundary conditions

In performing piezoelectric ceramic tests, the electric field between the electrodes is usually very high. Therefore, the specimens should be immersed in some dielectric media in order to prevent discharge. Thus, it can be assumed that the gap between the crack surfaces is filled with a homogenous dielectric medium that has the dielectric permittivity ε_m, and the electric displacement is continuous across the crack surfaces. Assume that the piezoelectric body contains a crack of contour denoted by Γ, and the outward unit normal is n. The crack is assumed to be filled with a homogeneous gas or liquid of dielectric permittivity ε_m, and is free of forces and surface charge density. Moreover, the mechanical and electrical loads in the form of forces, displacements, charge or voltages are applied to the body at remote distances. The body and crack regions are denoted by Ω and Ω^{c}, respectively. In the crack region, only the electric variables D^{c} and $E^{\mathrm{c}} = -\nabla\phi^{\mathrm{c}}$ exist, which can be determined from the solution of Laplace's equation for the electric potential, that is

$$\nabla^2\phi^{\mathrm{c}} = 0 \quad \text{in } \Omega^{\mathrm{c}}. \tag{37}$$

In turn, the electric displacement can be obtained by applying the constitutive relation

$$D^{\mathrm{c}} = \varepsilon_m E^{\mathrm{c}}. \tag{38}$$

Obviously, its normal component can be obtained from

$$D^{\mathrm{c}} \cdot n = -\varepsilon_m \frac{\partial\phi^{\mathrm{c}}}{\partial n}. \tag{39}$$

The exact boundary conditions are twofold: (a) the crack is traction free, and (b) on its contour the normal component of the induction and the electric potential are continuous. That is

$$T_j = 0, \qquad j = 1,2 \quad \text{on } \Gamma \tag{40}$$

$$D_n = -\varepsilon_m \frac{\partial\phi^{\mathrm{c}}}{\partial n}, \qquad \phi = \phi^{\mathrm{c}} \quad \text{on } \Gamma \tag{41}$$

where T_j are the Cartesian components of the stress vector. Three types of the commonly used electric boundary conditions, namely, the impermeable, permeable and conducting cracks, can be implemented using Eq. (41). For example, based on the fact that the dielectric constants of a ferroelectric ceramic are much larger than the one of air or vacuum (in fact, for most ceramics they can be about 3000 times larger), the electric boundary conditions of the so-called impermeable crack are approximated by

$$D_\theta^+ = D_\theta^- = 0, \quad \phi^+ = \phi^-, \tag{42}$$

which means the crack surfaces are free of surface charge and the crack is impermeable. For the permeable crack, based on Eq. (41), the following electrical crack surface boundary conditions can be expressed as [24,25]

$$D_\theta^+(u_\theta^+ - u_\theta^- + \Delta) = \varepsilon_m(\phi^- - \phi^+), \quad D_\theta^+ = D_\theta^- \tag{43}$$

where u_θ is the displacement component normal to the crack face, D_θ is the electric displacement component normal to the crack face, ϕ is the electrical potential and Δ is the distance between the upper and lower crack surfaces. The superscripts + and − denote the upper and lower surfaces of the crack, respectively. If there is no gap between the crack faces, i.e., $u_\theta^+ - u_\theta^- + \Delta = 0$, then Eq. (43) reduces to

$$D_\theta^+ = D_\theta^-, \quad \phi^+ = \phi^-. \tag{44}$$

When $u_\theta^+ - u_\theta^- + \Delta$ is a finite value and ε_m is very large, which means the medium between the crack surfaces becoming conducting, Eq. (43) can also reduce to Eq. (44). Therefore, Eq. (44) represents the case of conducting crack.

In order to consider the influence of CSEBC, an approach should be developed in the numerical procedure. The electric field in the gap between the crack surfaces can be depicted as

$$E_i = -\frac{\partial\phi}{\partial x_i}. \tag{45}$$

Since the gap distance is very small and the dielectric medium is homogenous, one can make the assumption that $\boldsymbol{E}$ is constant in the direction of the crack surface normal, which is the x_3 direction as shown in Fig. 2. Eq. (46) can then be written as

$$E_3^+ = E_3^- = -\frac{\phi^+ - \phi^-}{\Delta + u_3^+ - u_3^-} \tag{46}$$

and

$$D_3^+ = D_3^- = -\varepsilon_m \frac{\phi^+ - \phi^-}{\Delta + u_3^+ - u_3^-}. \tag{47}$$

Eq. (47) is the same as Eq. (43), which means that these two equations depict the same physical phenomenon. A dielectric finite element has been developed, by applying Eq. (45) first, to depict the electric field between the crack surfaces. In order to be identical to the system potential given by Eq. (9), the energy in the gap should be a negative one. Therefore, the total system potential, which includes those of the specimen and the dielectric medium between the crack surfaces, can be written as

$$\Pi^* = \Pi - \int_{V_m} \frac{1}{2}\boldsymbol{E}^{\mathrm{T}} \cdot \boldsymbol{d} \cdot \boldsymbol{E}\,\mathrm{d}V \tag{48}$$

in which V_m is the domain of the crack gap.

6. Numerical examples

In order to provide justification/validation for the proposed FEM, an example has been selected for the comparison of the proposed finite element and analytical solutions [35]. The specimen dimensions, finite element mesh and loading conditions are shown in Fig. 2, for the case of a centered elliptical cavity that is filled with a dielectric medium. If the material is poled along the x_3-direction, the material constant tensors, $\boldsymbol{C}$, $\boldsymbol{e}$ and $\boldsymbol{d}$, can be written as:

$$\boldsymbol{C} = \begin{bmatrix} C_{11} & C_{12} & C_{13} & 0 & 0 & 0 & 0 \\ C_{12} & C_{11} & C_{13} & 0 & 0 & 0 & 0 \\ C_{13} & C_{13} & C_{33} & 0 & 0 & 0 & 0 \\ 0 & 0 & 0 & C_{44} & 0 & 0 & 0 \\ 0 & 0 & 0 & 0 & 0 & C_{44} & 0 \\ 0 & 0 & 0 & 0 & 0 & 0 & \frac{1}{2}(C_{11} - C_{12}) \end{bmatrix}, \tag{49a}$$

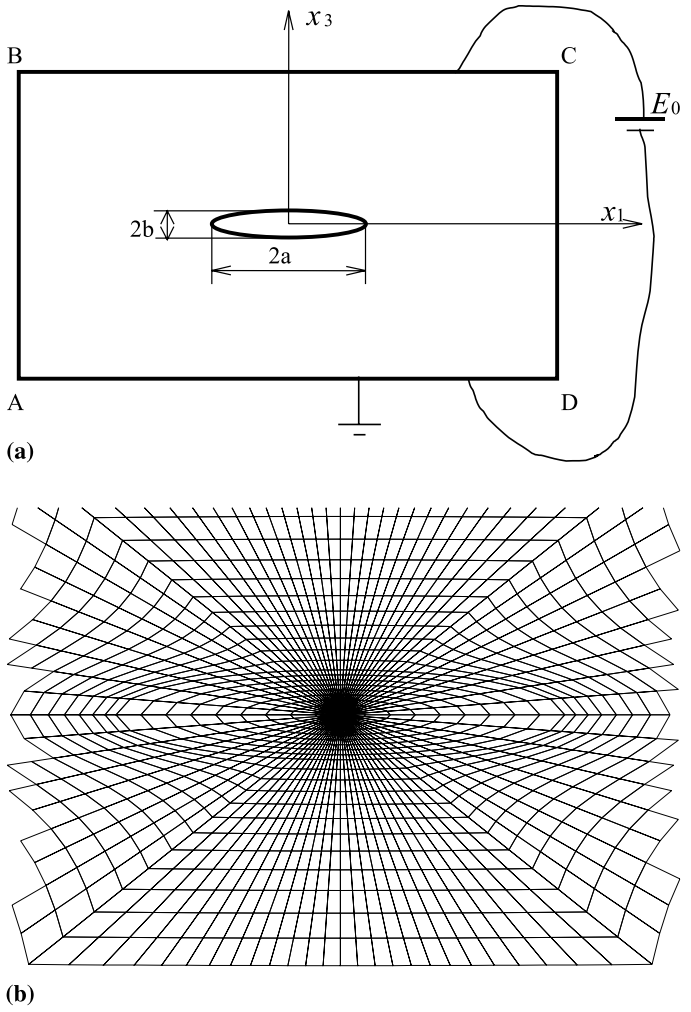

Fig. 2. Numerical model of a centered elliptical cavity in a large piezoelectric medium under combined mechanical-electrical loading in the x_3-direction: (a) schematic of the specimen with dimensions of $AB = 16$ m, BC $= 20$ m, $a = 1.0$ m, $b = 0.2$ m; (b) fine mesh around the cavity.

$$\boldsymbol{e} = \begin{bmatrix} 0 & 0 & 0 & 0 & e_{15} & 0 \\ 0 & 0 & 0 & e_{15} & 0 & 0 \\ e_{31} & e_{31} & e_{33} & 0 & 0 & 0 \end{bmatrix}, \tag{49b}$$

$$\boldsymbol{d} = \begin{bmatrix} d_{11} & 0 & 0 \\ 0 & d_{11} & 0 \\ 0 & 0 & d_{33} \end{bmatrix}. \tag{49c}$$

The material used is the PZT-4 ceramic with material constants:

$$C_{11} = 13.9 \times 10^{10}\ \mathrm{N/m^2}, \quad C_{12} = 7.78 \times 10^{10}\ \mathrm{N/m^2}, \quad C_{13} = 7.43 \times 10^{10}\ \mathrm{N/m^2},$$

$$C_{33} = 11.3 \times 10^{10}\ \mathrm{N/m^2}, \quad C_{44} = 2.56 \times 10^{10}\ \mathrm{N/m^2},$$

$$e_{31} = -6.98\ \mathrm{C/m^2}, \quad e_{33} = 13.84\ \mathrm{C/m^2}, \quad e_{15} = 13.44\ \mathrm{C/m^2},$$

$$\varepsilon_{11} = 6.0 \times 10^{-9}\ \mathrm{C/Vm}, \quad \varepsilon_{33} = 5.47 \times 10^{-9}\ \mathrm{C/Vm}.$$

In order to compare the proposed finite element results with the theoretical results obtained by Zhang et al. [35], the parameters used by them were selected for the present analysis. Thus, the dielectric constant of the medium inside the cavity, ε_m, was equal to 8.85×10^{-12} C/Vm. The major and minor semi-axes of the cavity, a and b, were equal to 1.0 and 0.2 m, respectively. The width and length of the specimen, i.e., lines AB and BC as shown in Fig. 2(a), were 16 and 20 m, respectively. As for the combined mechanical tensile and negative electric field loading in the x_3-direction, the tensile stress $\sigma^0 = 0.8$ MPa was applied on lines BC and AD, and the applied electric field was $E^0 = -50.0$ kV/m. Moreover, $\phi = 0.8$ MV was applied on line BC, and line AD was grounded to create E_0. Fig. 2(b) shows the fine finite element mesh around the cavity.

Convergence tests were carried out to assess the validity and quality of the numerical solution, before making a comparison with the corresponding theoretical results. Fig. 3 shows the results obtained using various meshes that employed different number of elements. The distributions of the electric field, E_3, ahead of an elliptical cavity versus distance, r, from the right apex of the ellipse are presented in Fig. 3(a). Whereas, the distributions of the stress, σ_{33}, ahead of an elliptical cavity vs distance, r, from the right apex of the ellipse are presented in Fig. 3(b). It can be clearly seen from Fig. 3 that the numerical results converged when the number of elements used was close to 5000.

Fig. 4(a) and (b) show the distributions of the stress, σ_{33}, and electric field, E_3, in front of the right major axial apex of an elliptical cavity, when the structure was subjected to a combined mechanical–electrical loading in the x_3-direction. As expected, both the stress and electric field concentrations are located at the apex of the cavity. The comparison of theoretical and FEM solutions for the distributions of E_3 and σ_{33} shows clearly that the proposed finite element results are in good agreement with the analytical results. Thus, the proposed finite element is accurate and reliable.

Next, we shall examine the effect of the electric boundary conditions of crack on the electro-mechanical field distributions near a crack. A double edge notched specimen, as shown in Fig. 5(a), of a piezoelectric ceramic (PZT-5H) was used for the numerical analysis in the present paper. The ratios of a/b and b/L are 0.5 and 0.2, respectively. Due to symmetry, only half of the specimen was modeled. For the mechanical boundary conditions, point C was fixed; and lines CD and AC were constrained in such a manner that they were only allowed to translate along x_1- and x_3-axes, respectively. For the electrical boundary conditions, line CD was grounded, which means that $\phi = 0$ at line CD. For the impermeable crack, no elements were used to mesh the crack gap and the boundary condition of no surface charge was adopted. Both the mechanical and electrical loads were applied on line AB. The material constants of PZT-5H are:

$$C_{11} = 12.6 \times 10^{10}\ \mathrm{N/m2}, \quad C_{12} = 5.5 \times 10^{10}\ \mathrm{N/m^2}, \quad C_{13} = 5.3 \times 10^{10}\ \mathrm{N/m^2},$$

$$C_{33} = 11.7 \times 10^{10}\ \mathrm{N/m^2}, \quad C_{44} = 3.53 \times 10^{10}\ \mathrm{N/m^2},$$

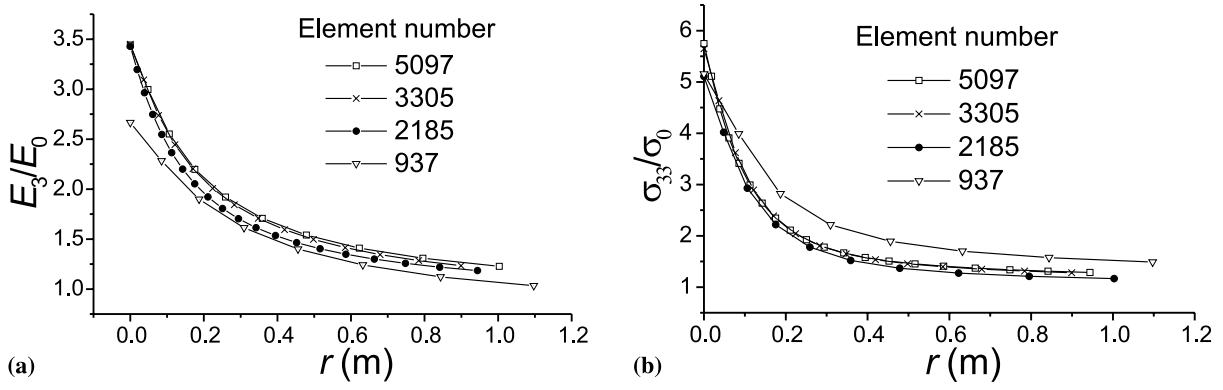

Fig. 3. Convergence testing: (a) distribution of electric field, E_3, ahead of an elliptical cavity vs distance, r, from the right apex of the ellipse; (b) distribution of stress, σ_{33}, ahead of an elliptical cavity vs. distance, r, from the right apex of the ellipse.

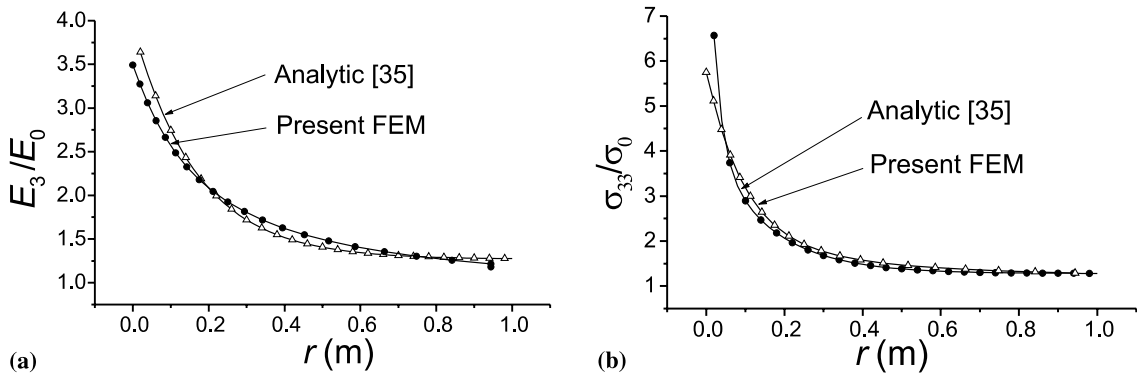

Fig. 4. Comparison of theoretical and FEM solutions: (a) distribution of electric field, E_3, ahead of an elliptical cavity vs distance, r, from the right apex of the ellipse; (b) distribution of stress, σ_{33}, ahead of an elliptical cavity vs distance, r, from the right apex of the ellipse.

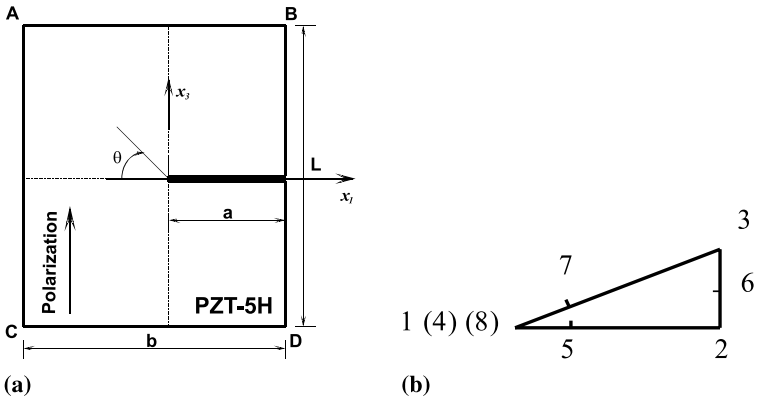

Fig. 5. Numerical model: (a) one half of a double edge notched specimen; (b) 6-nodes degenerated isoparametric singularity element.

$$e_{31} = -6.5\ \mathrm{C/m^2}, \quad e_{33} = 23.3\ \mathrm{C/m^2}, \quad e_{15} = 17.0\ \mathrm{C/m^2},$$

$$\varepsilon_{11} = 15.1 \times 10^{-9}\ \mathrm{C/Vm}, \quad \varepsilon_{33} = 13.0 \times 10^{-9}\ \mathrm{C/Vm}.$$

In Fig. 5(a), the crack surface is assumed to be perpendicular to the poling direction. For the electric load, when the applied electric field is in the same direction as that of polarization, which is parallel to the x_3-axis, it is deemed the positive applied electric field, and vice versa. In the present study, in order to create a positive (negative) electric field, a negative (positive) electric potential was applied on line AB. Hence, one can get a positive (negative) electric field E^0 defined as follows:

$$E^0 = \mp\phi/L. \tag{50}$$

A well-known 6-nodes degenerated isoparametric singular element, as shown in Fig. 5(b), which is often used in the elastic analysis [36], was employed to mesh the crack tip in the current model. With reference to Fig. 5(b), the element is degenerated from an 8-node isoparametric element. In order to create $1/\sqrt{r}$ singularity in the element, the mid-side nodes 5 and 7 are moved along the element edge to a quarter distance from the crack tip. Since the gap between the crack surfaces is very small and it is well known that a large ratio of element length to width will lead to unstable results, a small crack open angle $\alpha = 3^\circ$ was assumed in the present analysis. It was found that the stress and electric field distributions are almost identical at $\theta = 0^\circ$ in the case of impermeable crack. This shows that the proposed finite element results are accurate and reliable.

As an example, the notched specimen, as shown in Fig. 5(a), subjected to both an applied electric field and the combined mechanical tensile load and negative electric field, was analyzed. With regards to the applied electric field, a positive electric potential was applied on line AB to create a negative electric field. As for the combined loading, the applied mechanical tensile load was $\sigma^0 = 100\ \mathrm{N/m^2}$, and the applied negative electric field was varied. For a given ratio of electric field to mechanical load, γ, only three values of ε_m, i.e., 0.0, 0.1×10^{-9} and 0.1×10^{-8} C/Vm, were used for illustration to ensure clarity. Besides, the remanent polarization of the poled ceramic, $\bar{P}^{\mathrm{r}}$, was set to zero in the analyses. Since the stresses have the singularity of $1\sqrt{r}$, a factor $\kappa = \sqrt{2r/a}$ is used to normalize the stresses induced by either the applied electric field E^0 or the applied stress σ^0, as shown in Figs. 6 and 7.

Fig. 6 shows the variations of the normalized tangential stress with respect to angle θ near a crack, for different dielectric permittivities ε_m when the specimen was subjected to an applied negative electric field. It can be seen that as ε_m increases, the absolute maximum and minimum stresses decrease. This means that the stress singularity created by an electric field decreases with increasing ε_m. The appearance of stress singularity in the applied electric field is due to the fact that the electric field distributions in materials are inhomogeneous when a crack exists. However, the dielectric medium in the crack gap will decrease the inhomogeneity, therefore, the stress singularity decreases with increasing ε_m. When the dielectric permittivity of the medium in the crack gap is close to that of the piezoelectric material, the singularity will vanish. It seems that the increasing ε_m will decrease the impeding and enhancing effects on the crack propagation when a negative electric field is applied. The impermeable crack, which was commonly assumed by many researchers, is an extreme case, and it leads to the maximum singularities of the stress and electric displacement at the crack tip. Therefore, the impeding and enhancing effects of the applied electric field are overestimated in the case of impermeable crack.

Fig. 7(a) shows the distributions of the tangential stress σ_θ with respect to θ at the ratio of $\gamma = 2.0$ Vm/N. When $\varepsilon_m = 0.0$ C/Vm, which means that the crack is impermeable, the applied negative electric field tends to retard the crack propagation in the direction $\theta = 0^\circ$. But when the crack is permeable ($\varepsilon_m \neq 0.0$ C/Vm),

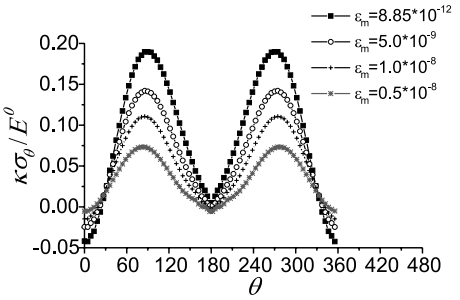

Fig. 6. The angular distributions of tangential stress under negative applied electric field.

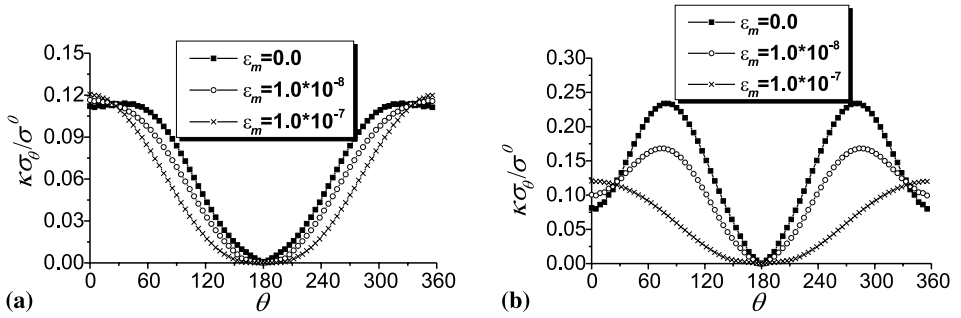

Fig. 7. Permeable crack under combined mechanical tensile load and negative electric field with variation of ε_m and (a) $\gamma = 2.0$ Vm/N, (b) $\gamma = 10.0$ Vm/N.

as the permittivity of the dielectric medium in the gap increases, the aforementioned effect decreases, as shown by the curves of $\varepsilon_m = 0.1 \times 10^{-9}$ C/Vm and $\varepsilon_m = 0.1 \times 10^{-8}$ C/Vm in Fig. 7(a). Furthermore, when ε_m is of the same order or larger than that of the piezoelectric ceramic, the retarding effect becomes so small that it can be omitted. Thus, the stress distributions near the crack tip are the same as those of the crack problem when only a mechanical tensile load is applied. Therefore, it may be concluded from the results in Fig. 7(a) that when the mechanical loading is dominant (i.e., the ratio, γ, is small), the effect of the permittivity of the dielectric medium in the gap on stress distributions near the crack is insignificant. Fig. 7(b) shows the distribution of the tangential stress σ_θ versus θ at the ratio of $\gamma = 10.0$ Vm/N. For $\varepsilon_m = 0.0$ C/Vm, the applied negative electric field tends to retard the crack propagation in the direction of $\theta = 0^\circ$ and enhances the propagation in the direction of $\theta = 0^\circ$. But from the curve of $\varepsilon_m = 0.1 \times 10^{-9}$ C/Vm, it can be seen that when the crack is permeable and as the permittivity of the dielectric medium in the gap increases, the enhancing effects also decrease. Besides, for $\varepsilon_m = 0.1 \times 10^{-8}$ C/Vm, one can find that when the ε_m is of the same order or larger than that of the ceramic, the retarding and enhancing effects become so small that it can be omitted. And the stress distributions near at the crack tip are identical to those in the case when only the mechanical tensile load is applied. It is obvious that when the electrical loading is dominant (i.e., the ratio, γ, is large), the effect of the permittivity of the dielectric medium in the gap on stress distributions near the crack is significant and the stress singularity is reduced by the increase of the ε_m in the gap.

7. Concluding remarks

In the present paper, a displacement-electric potential type finite element has been developed to analyze deformation and fracture of ferroelectric ceramic materials with defects. Based on the basic equilibrium equations, the electro-mechanical potential function is set-up that enables the FEM formulation. To account for the effect of depolarization in ferroelectrics, the constitutive equations have been modified for the remanent polarization, which, in turn, is employed in the FEM formulation. In addition, various electric boundary conditions on crack surfaces in ferroelectric ceramics are also considered in the finite element procedure developed. The convergence test was carried out to ascertain the mesh to be used for finite element analysis. The comparison of the theoretical and FEM solutions for the E_3 and σ_{33} distributions shows that the two solutions are in very good agreement. Thus, the proposed finite element is accurate and reliable.

As an example, the crack propagation of a double edge notched specimen of a PZT-5H ferroelectric ceramic with exact electric boundary conditions on the crack surfaces was analyzed. For the impermeable crack, when the combined mechanical tensile stress and negative electric field are applied, the electric field will impede the crack propagation in the direction $\theta = 0^\circ$ at a low ratio of electric potential to mechanical tension load. However, this electric field will tend to propagate the crack in an oblique direction more and more close to $\theta = 84^\circ$ as the aforementioned ratio increases. Therefore, the propagation direction is significantly dependent upon the loading ratio. For the permeable crack, it was found that the stress singularity will decrease due to the existence of the dielectric medium between the crack surfaces. The increasing ε_m will decrease the impeding and enhancing effects of the crack propagation in a negative applied electric field. The impeding and enhancing effects of the applied electric field will be overestimated when the impermeable crack model is adopted. When the permittivity of the dielectric medium in the crack gap is of the same order or larger than that of the ferroelectric ceramic, the crack tends to be a conducting crack and the applied electric field has no effect on the crack propagation. However, the effect of the permittivity of the dielectric medium in the gap on stress distributions near the crack is strongly dependent upon the loading ratio of the electrical load to the mechanical load. If the electrical loading is dominant (i.e., the ratio, γ, is large), the effect of the permittivity of the dielectric medium in the gap on stress distributions near the crack is significant and the stress singularity is reduced by the increase of the ε_m in the gap.

Note that only the maximum stress criterion was adopted in solving the numerical examples. A complete investigation of the behavior of crack propagation should involve both the maximum stress and energy release rate criteria. The work on searching a suitable energy release criterion is in progress, and the results will be published in near future. In addition, it is important to note that the presented FEM procedure is a linear one, which cannot analyze the hysteresis behavior of ferroelectric domain switching. The work on

nonlinear finite element analysis of ferroelectric materials, with the effects of ferroelectric and ferroelastic domain switching included, is also in progress and the results will be reported in near future.

Acknowledgements

Support from the National Natural Science Foundation of China under NNSFC grants #19672026 and #19891180 and from the State Education Commission of China is gratefully acknowledge.

References

[1] W.R.J.B. Cook, H. Jaffe, Piezoelectric Ceramics, Academic Press, London, 1971.
[2] T. Hao, X. Gong, Z. Suo, Fracture mechanics for the design of ceramic multilayer actuators, J. Mech. Phys. Solids 44 (1996) 23–48.
[3] V.Z. Parton, Fracture mechanics of piezoelectric materials, Acta Astronautica 3 (1976) 671–683.
[4] G.P. Cherepanov, Mechanics of Brittle Fracture, McGraw-Hill, New York, 1979, pp. 317–341.
[5] W.F. Deeg, The analysis of dislocation, crack and inclusion problems in piezoelectric solids, Ph.D. Thesis, Standford University, CA, USA, 1980.
[6] Y.E. Park, G. Hermann, Conservation laws and the material momentum tensor for the elastic dielectrics, Int. J. Eng. Sci. 24 (1986) 1365–1374.
[7] R.M. McMeeking, Electrostrictive forces near crack-like flaws, J. Appl. Math. Phys. 40 (1989) 615–627.
[8] R.M. McMeeking, A J-integral for the analysis of electrically induced mechanical stress at cracks in elastic dielectric, Int. J. Eng. Sci. 28 (1990) 605–613.
[9] Y. Pak, Crack Extension force in a piezoelectric material, J. Appl. Mech. 67 (1990) 647–653.
[10] H. Sosa, Plane problem in piezoelectric media with defects, Int. J. Solid. Struct. 28 (1991) 491–505.
[11] H. Sosa, Y. Pak, Three dimensional eigenfunction analysis of a crack in a piezoelectric material, Int. J. Solid. Struct. 26 (1990) 1–15.
[12] Z. Suo, C.M. Kuo, D.M. Barnet, J.R. Willis, Fracture mechanics for piezoelectric ceramics, J. Mech. Phys. Solids 40 (1992) 739–765.
[13] Z. Suo, Models for breakdown-resistant dielectric and ferroelectric ceramics, J. Mech. Phys. Solids 41 (1993) 1156–1176.
[14] B. Wang, Three-dimensional analysis of a flat elliptical crack in a piezoelectric material, Int. J. Eng. Sci. 6 (1992) 191–781.
[15] M.L. Dunn, The effects of crack face boundary conditions on the fracture mechanics of piezoelectric solids, Eng. Fract. Mech. 48 (1994) 25–39.
[16] S. Kumar, R.N. Singh, Crack propagation in piezoelectric materials under combined mechanical and electrical loading, Acta Mater. 44 (1996) 173–200.
[17] S.B. Park, C.T. Sun, Fracture criteria for piezoelectric ceramics, J. Am. Ceram. Soc. 78 (1995) 1475–1480.
[18] T.Y. Zhang, P. Tong, Fracture mechanics for a mode III crack in a piezoelectric material, Int. J. Solids Struct. 33 (1996) 343–359.
[19] H.J. Gao, T.Y. Zhang, P. Tong, Local and global energy release rates for an electrically yielded crack in a piezoelectric ceramic, J. Mech. Phys. Solids 45 (1997) 491–510.
[20] X. Wang, Y. Shen, Some basic theory for thermal magnetic electric elastic media, Chinese J. Appl. Mech. 12 (1995) 28–39 in Chinese.
[21] C.L. Hom, N. Shankar, A numerical analysis of relaxor ferroelectric multilayered actuators and 2-2 composite arrays, J. Smart Mater. Struct. 4 (1995) 266–273.
[22] C.L. Hom, N. Shankar, A fully coupled constitutive model for electrostrictive ceramic materials, J. Int. Mater. Syst. Struct. 5 (1994) 795–801.
[23] S. Kumar, R.N. Singh, Energy release rate and crack propagation in piezoelectric materials Part II: Combined mechanical and electrical loads, Acta Mater. 45 (1997) 859–868.
[24] T.H. Hao, Z.Y. Shen, A new electric boundary condition of electric fracture mechanics and its applications, Eng. Fract. Mech. 47 (1994) 793–802.
[25] H. Sosa, N. Khutoryansky, New developments concerning piezoelectric materials with defects, Int. J. Solids Struct. 33 (1996) 3399–3414.
[26] M.E. Lines, A.M. Glass, Principles and Applications of Ferroelectrics and Related Materials, Oxford University Press, Oxford, 1977.
[27] D. Berlincourt, Piezoelectric ceramics: characteristics and applications, J. Acoust.Soc.Am. 70 (1991) 1586–1595.
[28] H.H.A. Krueger, Stress sensitivity of piezoelectric ceramics. Part 1: Sensitivity to compressive stress parallel to the polar axis, J. Acoust. Soc. Am. 42 (1967) 636–645.
[29] C.S. Lynch, The effect of uniaxial stress on the electro-mechanical response of 8/6/35 PLZT, Acta Mater. 44 (1996) 4137–4148.
[30] S.C. Hwang, X.C.S. Lynch, R.M. McMeeking, Ferroelectric/ferroelastic interactions and a polarization switching model, Acta Metall. Mater. 43 (1995) 2073–2084.
[31] H.C. Cao, A.G. Evans, Nonlinear deformation of ferroelectric ceramics, J.Am.Ceram.Soc. 76 (1993) 890–896.

[32] X. Chen, D.N. Fang, K.C. Hwang, Micromechanics simulation of ferroelectric polarization switching, Acta Mater. 45 (1997) 3181–3189.
[33] W. Lu, D.N. Fang, K.C. Hwang, Numerical analysis of ferroelectric/ferroelastic domain switching in ferroelectric ceramics, Comput. Mater. Sci. 8 (1997) 291–308.
[34] W. Lu, D.N. Fang, K.C. Hwang, A constitutive theory for ferroelectric ceramics, Key Eng. Mater. 145 (1997) 983–989.
[35] T.Y. Zhang, C.F. Aian, P. Tong, Linear electro-elastic analysis of a cavity or a crack in a piezoelectric material, Int. J. Solids Struct. 35 (1998) 2121–2149.
[36] T.L. Anderson, Fracture Mechanics: Fundamentals and Applications, CRC Press, Boston, 1991.